



Band-like transporting and thermally durable V-shaped organic semiconductors with a phenyl key block

Journal:	<i>Journal of Materials Chemistry C</i>
Manuscript ID	TC-ART-07-2020-003318.R1
Article Type:	Paper
Date Submitted by the Author:	31-Aug-2020
Complete List of Authors:	Sawabe, Chizuru; The University of Tokyo, Department of Advanced Materials Science, Graduate School of Frontier Sciences Kumagai, Shohei; The University of Tokyo, Department of Advanced Materials Science Mitani, Masato; The University of Tokyo, Graduate School of Frontier Sciences Ishii, Hiroyuki; University of Tsukuba Yamagishi, Masakazu; National Institute of Technology, Toyama College Sagayama, Hajime; Institute of Materials Structure Science, High Energy Accelerator Research Organization Kumai, Reiji; High Energy Accelerator Research Organization (KEK) , Institute of Materials Structure Science Sato, Hiroyasu; Rigaku Corporation, Takeya, Jun; The University of Tokyo, Department of Advanced Materials Science Okamoto, Toshihiro; The University of Tokyo, Department of Advanced Materials Science, School of Frontier Sciences

ARTICLE

Band-like transporting and thermally durable V-shaped organic semiconductors with a phenyl key block

Received 00th January 20xx,
Accepted 00th January 20xx

Chizuru Sawabe,^a Shohei Kumagai,^a Masato Mitani,^a Hiroyuki Ishii,^b Masakazu Yamagishi,^c Hajime Sagayama,^d Reiji Kumai,^d Hiroyasu Sato,^e Jun Takeya^{a,f,g} and Toshihiro Okamoto^{*,a,f,h}

DOI: 10.1039/x0xx00000x

Towards the development of high-performance small molecule-based organic semiconductors with high carrier mobility and high thermal durability, strategic and systematic investigations are needed for not only molecular design of π -electron cores and substituents but also fundamental and structural analyses. Here, we focus on the sulphur-containing V-shaped π -electron systems with phenyl substituents and carry out comprehensive analyses of molecular assembly and charge-transport properties. Phenyl- and decyl-phenyl-substituted **DNT-Vs** (**Ph-DNT-VW** and **C₁₀Ph-DNT-VW**) are readily synthesized through a versatile synthetic procedure. Single crystal data and their theoretical calculations suggested that both compounds form typical herringbone-type packing structures that are favorable for two-dimensional charge-transporting capability. Indeed, single-crystal transistors of **Ph-DNT-VW** and **C₁₀Ph-DNT-VW** have excellent mobility of 3.1 and 8.1 cm² V⁻¹ s⁻¹. Furthermore, their negative temperature coefficients of mobility strongly suggest band-like transport characteristics. Finally, solution-processed thin-film transistors of **C₁₀Ph-DNT-VW** exhibit high thermal durability up to 180 °C, which is an essential feature for practical electronics.

Introduction

Organic semiconductors (OSCs) have attracted much attention as the key materials for next-generation organic-based electronics¹⁻⁴ due to their mechanical flexibility, lightweight, and potential solution processability originating from molecular assemblies *via* weak van der Waals interactions. For future applications, OSCs are required to have 1) high carrier mobility, 2) solution processability and 3) stability against ambient and thermal stresses. Since carrier transports for OSCs have been depicted by the hopping transport mechanism based on the Marcus theory,⁵ OSCs are designed to possess small reorganization energies (λ) and large transfer integrals (t)

between neighbouring molecules in the solid states. On the other hand, the band-like transport mechanism in OSCs has attracted intense attention since early works on high-performance rubrene in single-crystal organic field-effect transistors (OFETs).⁶⁻⁸ Thus, the band-like transport system is currently considered as a promising feature for realizing high carrier mobility. Likewise, large t is essential for the band-like transport.⁹ In addition, suppression of molecular motions is necessary for the band-like transport to reduce carrier scatterings caused by vibrations (or referred as dynamic disorder).^{8, 10, 11} The new molecular design approach based on molecular orbital engineering was developed to minimize the variation of t (Δt) caused by the molecular motions.¹² Besides, technical developments of single-crystal OFETs,¹³⁻¹⁹ which can ignore negative influences of grain boundaries, are of additional importance for effective application of the band-like transport

^a Material Innovation Research Center (MIRC) and Department of Advanced Materials Science, School of Frontier Sciences, The University of Tokyo, 5-1-5 Kashiwanoha, Kashiwa, Chiba 277-8561, Japan.

^b Department of Applied Physics, Faculty of Pure and Applied Sciences, University of Tsukuba, 1-1-1 Tennodai, Tsukuba, Ibaraki 305-8573, Japan.

^c National Institute of Technology, Toyama College, 13 Hongo-machi, Toyama, Toyama 939-8630, Japan.

^d Condensed Matter Research Centre (CMRC) and Photon Factory, Institute of Materials Structure Science, High Energy Accelerator Research Organization (KEK), Tsukuba, Ibaraki 305-0801, Japan.

^e Rigaku Corporation, 3-9-12 Matsubara-cho, Akishima, Tokyo 196-8666, Japan.

^f National Institute of Advanced Industrial Science and Technology (AIST)-University of Tokyo Advanced Operando-Measurement Technology Open Innovation Laboratory (OPERANDO-OIL), AIST, 5-1-5 Kashiwanoha, Kashiwa, Chiba 277-8561, Japan.

^g International Center for Materials Nanoarchitectonics (MANA), National Institute for Materials Science (NIMS), 1-1 Namiki, Tsukuba, Ibaraki 305-0044, Japan.

^h PRESTO, JST, 4-1-8 Honcho, Kawaguchi, Saitama 332-0012, Japan.

*Electronic supplementary information (ESI) available. CCDC 2010669 (Ph-DNT-VW), 2010670 (C₁₀Ph-DNT-VW) and 2010721 (C₁₀-DNT-VW). For ESI and crystallographic data in CIF or other electronic format see DOI: 10.1039/x0xx00000x

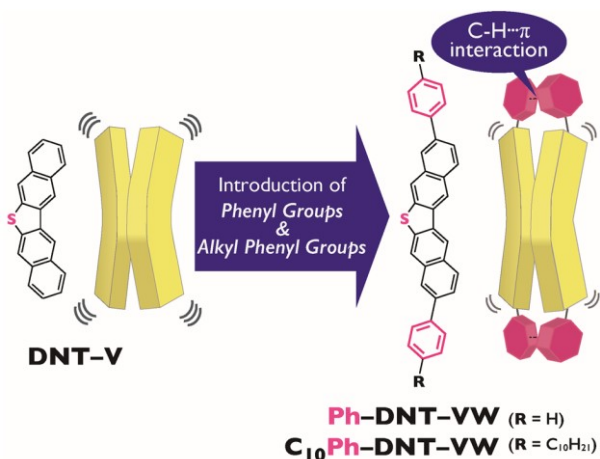


Fig. 1 Molecular design.

to actual devices. Thermal stability on devices is often derived from the thermodynamic properties of OSCs, such as crystal-to-crystal, crystal-to-liquid-crystal phase transitions, melting and sublimation at elevated temperatures. The stability of the preferred crystal phase for carrier transport depends on the intermolecular interactions and the molecular weight. To produce solution processable OSCs, flexible alkyl groups are often employed as substituents. However, such flexible moieties are concomitantly linked to possible thermal instability. Therefore, molecular design strategies by means of both π -electron cores and substituents are critically required to achieve solution-processability and thermal stability at the same time.

In recent years, our group has developed a series of bent-shaped π -cores, aiming at effective intermolecular orbital overlaps and the suppression of molecular motions towards high carrier mobility, solution processability and sufficient thermal durability.⁴ For instance, the sulphur-bridged dinaphtho[2,3-*b*;2',3'-*d*]thiophene (**DNT-V**) V-shaped derivatives²⁰ exhibit 1) large t values via S... π interactions arising from large orbital coefficient at the sulphur atoms, 2) high solubility owing to the permanent dipole moment of the V-shaped molecule,²¹ and 3) enhanced stability of the crystal phase due to suppression of molecular motions attributed to the aggregation-induced non-planar geometry. In particular, alkyl-substituted **C_n-DNT-VW** ($n = 6, 10$) were successfully applied to solution-processed single-crystal OFETs with the maximum hole mobility of $9.5 \text{ cm}^2 \text{ V}^{-1} \text{ s}^{-1}$ and device durability up to $150 \text{ }^\circ\text{C}$. As such, the bent-shaped π -cores represented by **DNT-V** have been shown as promising platforms for practical OSCs compared to traditional linear or quasi-linear π -cores, such as pentacene²², [1]benzothieno[3,2-*b*][1]benzothiophene (**BTBT**)²³ and dinaphtho[2,3-*b*:2',3'-*f*]thieno[3,2-*b*]thiophene (**DNTT**),²⁴ especially in terms of thermal durability on devices. However, device performance of **C₆-DNT-VW**-based transistor was found consistent only up to $150 \text{ }^\circ\text{C}$, which was lower than the phase transition point of $202 \text{ }^\circ\text{C}$ due to its low molecular weight, resulting in insufficient thermal durability. In addition, replacing hexyl with decyl groups on **DNT-VW** led to a lower phase transition temperature of $151 \text{ }^\circ\text{C}$. Thus, alkyl substituents

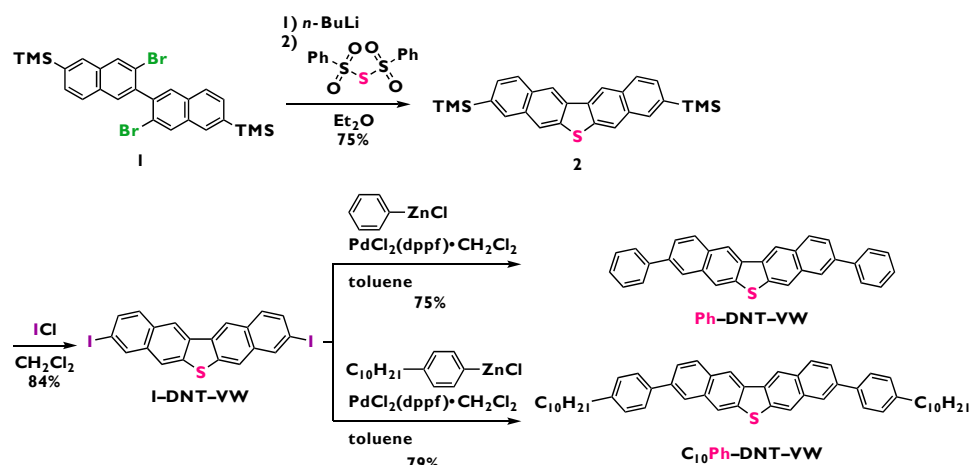
could lead to a trade-off between thermal durability and carrier mobilities. Therefore, it should be important to investigate a new class of substituents for OSCs that not only enable high carrier mobility and solution process but also provide excellent thermal durability. Phenyl group is known as a rigid functional group in OSCs, which tunes aggregated structures *via* C-H... π interactions and improves thermal durability. However, the phenyl group itself lowers the solubility of OSCs and solution-processability.

Herein, we have developed a phenyl-based thermally durable substituent with *para*-functionalization by an alkyl group. To assess the individual roles of phenyl and alkyl moieties in crystal structures, thermal properties, as well as charge transporting mechanism and capability, two derivatives with phenyl (**Ph-DNT-VW**) and *p*-decylphenyl (**C₁₀Ph-DNT-VW**) functional groups along with a non-substituted and decyl derivative (**DNT-V** and **C₁₀-DNT-VW**) were prepared and investigated comparatively. From the results of single-crystal structural analyses, the phenyl moiety was regarded as a fine-tuning element of aggregated structures and acted to enhance the planarity of the π -core, while the alkyl moiety could lead to closer packing of **DNT-V** π -cores due to its flexibility. By means of variable-temperature measurements of single-crystal OFETs prepared by either physical-vapor transporting (PVT)- or solution-crystallization techniques, all four derivatives were found to follow the band-like transport model. Accordingly, the crystal structures were evaluated from the viewpoint of band transport mechanism, *i.e.*, theoretical calculations of effective mass and concomitant speculations of carrier scattering caused by the dynamic disorder, where the alkyl moiety was likely preferable for reducing dynamic disorder. On the other hand, phenyl and decylphenyl moieties effectively improved thermal durability in the OFET state. Therefore, we show that the alkylphenyl groups possess the potential to achieve high carrier mobility with band-like transport, solution processability and high thermal durability for OSCs.

Results and discussion

Synthesis

In the synthetic scheme of alkyl-substituted **DNT-V** derivatives



Scheme 1 Synthetic route to the **DNT-V** derivatives used in this study.

reported in the previous paper, corresponding alkyl-substituted 2-methoxynaphthalenes were required as the starting material.²⁰ To improve the synthetic efficiency for derivatization,²⁵ we developed a more versatile synthetic route. As the key precursor, we synthesized an iodine-substituted **DNT-V** (**I-DNT-VW**) to readily enable introductions of various functional groups by cross-coupling reactions (Scheme 1). A halogen-lithium exchange of **1**, followed by a cyclization using benzenesulfonic thioanhydride as an electrophilic sulphur, afforded 3,9-bis(trimethylsilyl)dinaphtho[2,3-*b*:2',3'-*d*]thiophene (**2**). Iodination of **2** by iodine chloride yielded **I-DNT-VW**. **Ph-DNT-VW** and **C₁₀Ph-DNT-VW** were obtained in good yields by the Negishi coupling reaction of **I-DNT-VW** with phenyl zinc chloride and *p*-decylphenyl zinc chloride, respectively. The target compounds were further purified by recrystallization and sublimation prior to fundamental analysis and device evaluations.

Chemical and thermal stabilities

Chemical and thermal stabilities of the current **DNT-V** derivatives were evaluated by time-dependent UV-vis (TD-UV-vis) absorption spectra of vacuum-deposited thin films and thermogravimetric-differential thermal analysis (TG-DTA). The TD-UV-vis absorption spectra for **Ph-DNT-VW** and **C₁₀Ph-DNT-VW** remained unchanged under ambient atmosphere for over one week, indicating their excellent air stabilities (Figure S1 and S2). TG-DTA showed no thermal decompositions below the 5%-weight-loss temperatures ($T_{95\%}$) of 389 °C and 432 °C for **Ph-DNT-VW** and **C₁₀Ph-DNT-VW**, respectively (Figure S3), which are higher than those of unsubstituted **DNT-V** (266 °C) and **C₁₀-DNT-VW** (367 °C). Thus, **Ph-DNT-VW** and **C₁₀Ph-DNT-VW** possess high thermal stability, which allows for purification by sublimation.

Crystal structures and transfer integrals

Single-crystal X-ray structure determinations were carried out for **Ph-DNT-VW** and **C₁₀Ph-DNT-VW** at room temperature. In addition, the crystal structure of **C₁₀-DNT-VW** was revisited, providing an improved understanding of the aggregated structure of **DNT-V** derivatives.²⁰ Thin plate-like single crystals of three compounds were obtained from solutions. Figure 2

shows molecular and packing structures of **DNT-V** derivatives. All **DNT-V** derivatives formed the layer-by-layer herringbone-type packing motifs which are favourable for effective two-dimensional charge-carrier transport.⁴ In terms of the molecular structures, **DNT-V** π -cores in **Ph-DNT-VW** and **C₁₀Ph-DNT-VW** along with **C₁₀-DNT-VW** show a non-planar conformation, while the optimization of their molecular geometries by density

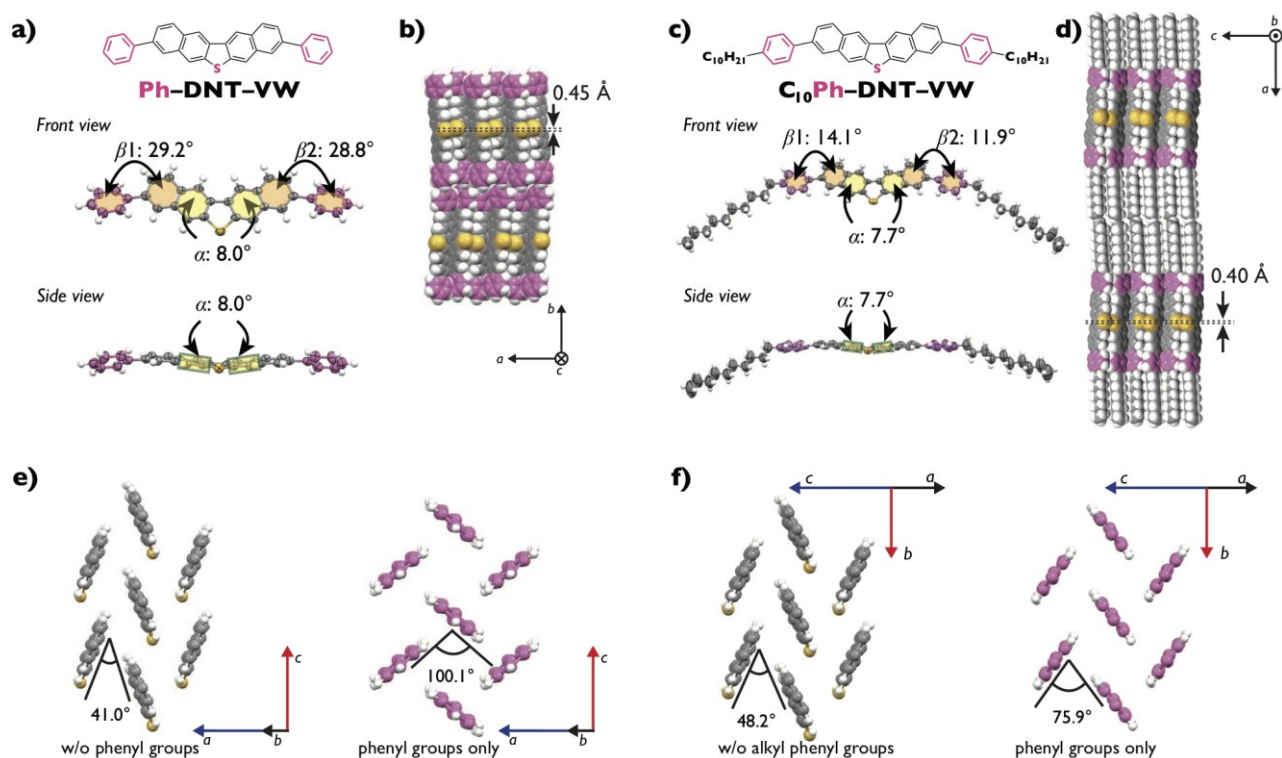


Fig. 2 Molecular structures of a) **Ph-DNT-VW** and c) **C₁₀Ph-DNT-VW** in the single crystal. Lamellar structures in *ab*(or *ac*)-plane and a displacement in the adjacent two molecules of b) **Ph-DNT-VW** and d) **C₁₀Ph-DNT-VW**. Angles between **DNT-V** cores (left) and angles between phenyl groups (right) in assembled structures of e) **Ph-DNT-VW** and f) **C₁₀Ph-DNT-VW**.

functional theory (DFT) calculation provided a completely planar conformation. Hence, the non-planar conformation of **DNT-V** core is a unique feature triggered by aggregation-induced intermolecular interactions in the solid states.^{4, 20, 26}

The non-planarity is quantified by the bent angle between naphthalene rings (α), and α values are found to be 13.9° and 13.3° for the non-substituted **DNT-V** and **C₁₀-DNT-VW**, respectively, while **Ph-DNT-VW** and **C₁₀Ph-DNT-VW** show α of 8.0° and 7.7°, respectively (Figure 2a, c). Besides, the dihedral angles between the outer benzene ring and the phenyl functional group (β_1/β_2) were 29.2°/28.8° and 14.1°/11.9° for **Ph-DNT-VW** and **C₁₀Ph-DNT-VW**, respectively. Note that the phenyl groups between neighbouring molecules interact with each other *via* the C-H \cdots π interactions in a herringbone-type packing motif, which is likely competitive with the alignment of the **DNT-V** cores. Therefore, it is suggested that the aggregation-induced non-planarity of **DNT-V** π -cores is tuneable by introducing rigid or bulky functional groups which can strongly interact with themselves.

The herringbone packings of **DNT-V** cores are supported by the core-to-core interactions such as short C-H \cdots π and S \cdots π (Figure S8 and Figure S9). For example, **Ph-DNT-VW** possesses several short contacts in the *ac*-plane (Figure S8): short S \cdots C contacts (S1 \cdots C7: 3.33 Å, S1 \cdots C12: 3.41 Å) due to the S \cdots π interaction observed between the inner thiophenes in a head-to-head (HH) dimer, whereas short C \cdots H contacts between the inner benzene rings (C10 \cdots H45: 2.73 Å, C18 \cdots H45: 2.88 Å) are observed in a tail-to-tail (TT) dimer. Consistent intermolecular

interactions are commonly found in all **DNT-V** derivatives studied herein, indicating tightly packed structures and effective overlaps of molecular orbitals.

Calculation of *t* values between the highest occupied molecular orbitals (HOMOs) of neighbouring molecules resulted in the similar values in the HT and HH dimers regardless of the functional groups, whereas the absolute *t* values in the TT dimers of **Ph-DNT-VW** and **C₁₀Ph-DNT-VW** were more than twice as large as that of **DNT-V** (**Ph-DNT-VW**: -33 meV, **C₁₀Ph-DNT-VW**: -32 meV, **DNT-V**: -13 meV) and similar value to that of **C₁₀-DNT-VW** ($t_{TT} = -35$ meV) (Table 1). Although the **DNT-V** derivatives showed similar packing structures, longitudinal displacements in adjacent two molecules of both **Ph-DNT-VW** and **C₁₀Ph-DNT-VW** (Figure 2b and d, 0.45 Å and 0.40 Å, respectively) were smaller than that of **DNT-V** (0.99 Å) (Figure S10). Note that an absent of the displacement in **C₁₀-DNT-VW** (Figure S10) led to the largest absolute *t* in the TT dimer (Table 1). Thus, the phenyl group could more dominantly fix the longitudinal displacements of π -cores, while the alkyl group itself could reduce the displacement due to its flexibility contrary to π -conjugated cores.

Device evaluations and band calculations

Single-crystalline OFET properties of **Ph-DNT-VW** and **C₁₀Ph-DNT-VW** were evaluated (Figures 3 and S14). Owing to the low solubility of **Ph-DNT-VW** (<0.0005 wt% in 3-phenoxytoluene at 80 °C) (Table S3), its single-crystalline films were prepared by means of physical vapor transport, whereas

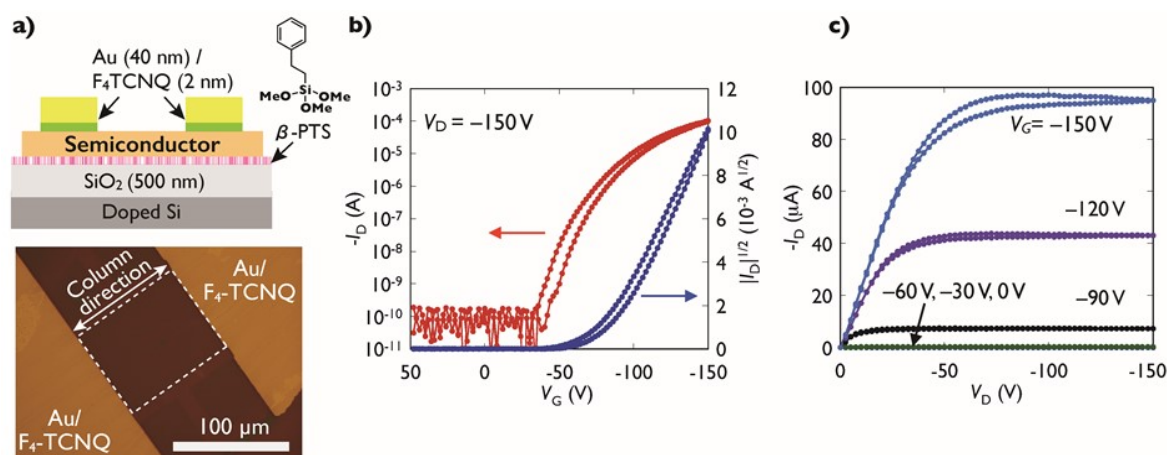


Fig. 3 a) Device structure and microscopic image, b) transfer characteristics and c) output characteristics of the device using $C_{10}Ph-DNT-VW$ single crystalline film.

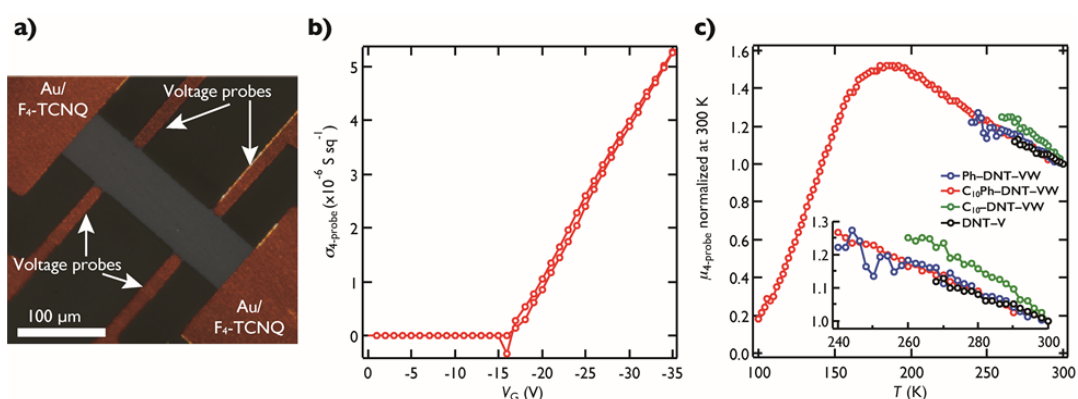


Fig. 4 a) Microscopic image, b) sheet conductivity ($\sigma_{4-probe}$) as a function of V_G of the four-probe device using $C_{10}Ph-DNT-VW$ single crystalline film. c) Temperature-dependence of mobility evaluated by the four-probe device using single crystalline films of $DNT-V$ derivatives. Inset: magnification of the range of 240–300 K.

solution-processed edge-casting method¹³ was applied to the soluble $C_{10}Ph-DNT-VW$ derivative. The OFETs were prepared in the bottom-gate/top-contact device architecture, and 2,3,5,6-tetrafluoro-7,7,8,8-tetracyanoquinodimethane (F_4-TCNQ) was used as a contact dopant to improve hole injection into the OSC layer.²⁷ All OFET channels were aligned parallel to the column direction of the herringbone structure (Figure 2), which was verified by transmission X-ray diffraction analysis (Figure S14c and S15c). Hole mobility in the saturation regime was referred as two-probe mobility ($\mu_{2-probe}$). The maximum $\mu_{2-probe}$ was 3.1 and 8.1 $cm^2 V^{-1} s^{-1}$ for $Ph-DNT-VW$ and $C_{10}Ph-DNT-VW$, respectively (Figures S14 and 3, and Table 1). It is not trivial to simply correlate $\mu_{2-probe}$ and t values of $DNT-V$ derivatives. Besides, carrier mobility could be either over- or underestimated due to general contact resistance issue,^{28, 29} where Schottky barrier between OSC and metal electrodes³⁰ and access resistance through the bulk OSC region dependent on OSC film thickness^{16, 31} could disturb the appearance of intrinsic mobility of OSCs. A four-probe OFET measurement, hence, is appropriate to estimate the intrinsic carrier mobility. Indeed, $C_6-DNT-VW$ was studied both with the two- and four-probe methods in the previous work, resulting in a higher four-probe mobility ($\mu_{4-probe}$) than $\mu_{2-probe}$.²⁰ Then, four-probe OFETs were prepared based on the four $DNT-V$

derivatives (Figure 4 and S16-S19). $\mu_{4-probe}$ was extracted from the slope of four-probe sheet conductivity ($\sigma_{4-probe}$) (Figure 4b). As summarized in Table 1, the maximum $\mu_{2-probe}$ and $\mu_{4-probe}$ are almost consistent with each other, whereas $C_{10}Ph-DNT-VW$ shows $\mu_{4-probe}$ of 9.7 $cm^2 V^{-1} s^{-1}$, higher than the maximum $\mu_{2-probe}$ of 6.5 $cm^2 V^{-1} s^{-1}$. Therefore, the $\mu_{4-probe}$ results in the following order: $C_{10}Ph-DNT-VW$ (9.7 $cm^2 V^{-1} s^{-1}$) > $C_{10}Ph-DNT-VW$ (8.1 $cm^2 V^{-1} s^{-1}$) > $Ph-DNT-VW$ (3.0 $cm^2 V^{-1} s^{-1}$) > $DNT-V$ (1.7 $cm^2 V^{-1} s^{-1}$). Here, one may be aware that $DNT-V$ derivatives with decyl substituents exhibit higher mobilities than non-alkylated derivatives, and the trend will be discussed in later section. In addition, temperature dependences of $\mu_{4-probe}$ were investigated on four-probe OFETs. As shown in Figure 4c, all $DNT-V$ derivatives showed an increase in $\mu_{4-probe}$ with decreasing temperature down to 180 K for $C_{10}Ph-DNT-VW$ and to 240–268 K for the others, the latter of which corresponds to temperatures at which the devices got wrong probably due to cracks. The negative temperature (T) dependence of $\mu_{4-probe}$ ($\partial\mu_{4-probe}/\partial T$) indicates a band-like carrier transport, where the increase in mobility could be attributed to suppressed carrier scattering from molecular motions at lowered temperatures.^{7, 11} Besides, according to the multiple trap-and-release model,^{7, 32} the decrease in $\mu_{4-probe}$ value of $C_{10}Ph-DNT-VW$ below 180 K is attributed to carrier trapping behaviours by shallow traps.

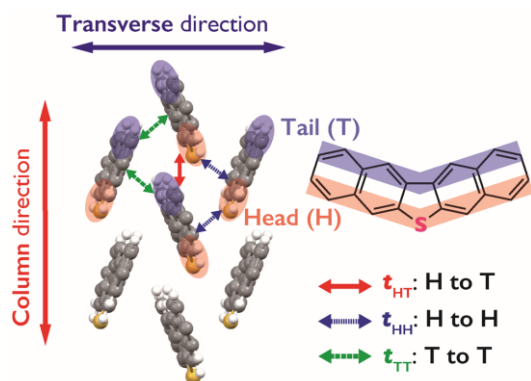


Fig. 5 Definitions of transfer integrals and column/transverse direction in the herringbone packing structure of **DNT-V** derivatives. The crystal structure of **Ph-DNT-VW** is illustrated as a representative, where phenyl groups are omitted for clarity.

Correlations between mobility and crystal structure are then revisited by the band transport model:

$$\mu = q\tau/m^*$$

where q stands for the elementary charge, τ is the average relaxation time of mobile carrier, and m^* denotes the effective mass of carrier. For estimating m^* , band structures of four **DNT-V** derivatives were calculated by using a plane-wave basis with the vdW-DF2 functional³³ as implemented in the Quantum ESPRESSO (Figure S11-S13).³⁴ Effective masses along the column direction (m_{\parallel}^*) and transverse direction (m_{\perp}^*) were estimated from curvatures of the band dispersion on the top of the valence band. As shown in Table 1, most m_{\parallel}^* are smaller than m_{\perp}^* for each compound, which indicates preferable hole transport along the column direction. A clear and consistent relationship between m_{\parallel}^* and $\mu_{4\text{-probe}}$ is found in the comparison of **DNT-V** with **C₁₀-DNT-VW**: **C₁₀-DNT-VW** with the smallest m_{\parallel}^* exhibits the highest $\mu_{4\text{-probe}}$ while **DNT-V** reveals the opposite trend. However, **Ph-DNT-VW** and **C₁₀Ph-DNT-VW** gave the same m_{\parallel}^* of $2.3m_0$ (m_0 is the electron rest mass), although their $\mu_{4\text{-probe}}$ were 2.7 times different. This probably originates from the reduction of molecular motions along the molecular long axis caused by the alkyl substituents as reported by Illig *et al.* by using transmission electron microscopy (TEM).¹⁰ The highest $\mu_{4\text{-probe}}$ of **C₁₀-DNT-VW** may also be linked to the same origin. Future work by TEM, inelastic neutron scattering³⁵ and terahertz Raman spectroscopy³⁶ would provide understanding of impacts of phenyl and alkylphenyl substituents on molecular motions related to carrier transport.

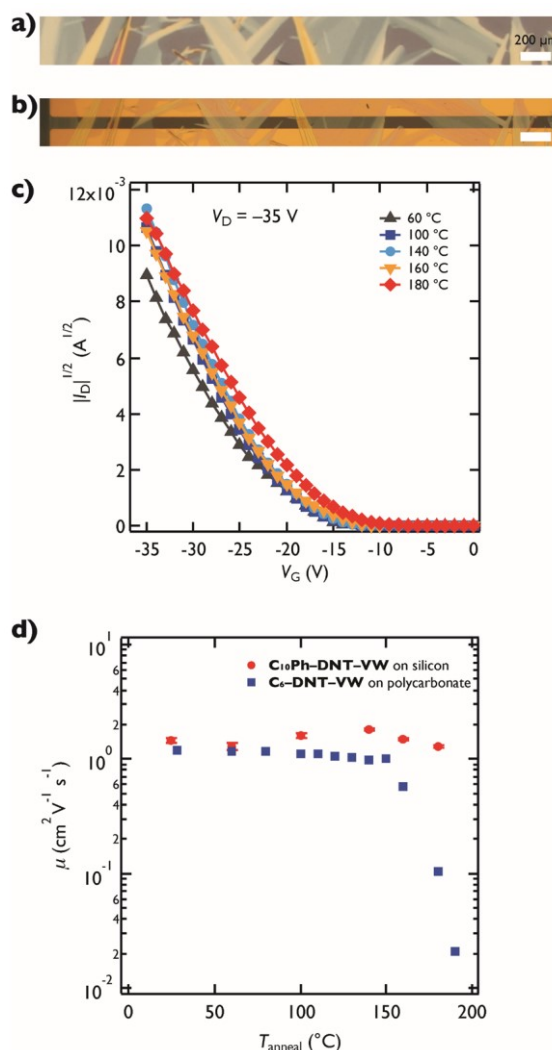


Fig. 6 Microscopic images of **C₁₀Ph-DNT-VW** single crystalline film a) before 180 °C treatment and b) after 180 °C treatment and device fabrication. c) Transfer characteristics of the annealed-single-crystal transistor of **C₁₀Ph-DNT-VW** after each annealing process at various temperatures. d) Mobility plots of **C₁₀Ph-DNT-VW** on silicon substrate and **C₆-DNT-VW** on polycarbonate²⁰ vs treatment temperature. For **C₁₀Ph-DNT-VW**, the error bars represent the standard deviation of mobility values at high gate voltage region.

Thermal durability

Thermal durability of solution-processed OFETs based on **C₁₀Ph-DNT-VW** were studied to verify the advantage of alkylphenyl group. In the previous work, thermal stress measurements were performed on **C₆-DNT-VW**, revealing a thermal durability up to 150 °C by using a polycarbonate

Table 1 Transfer integral, effective mass and mobility for the **DNT-V** derivatives.

Material	Transfer integral, t [meV]			Effective mass		Mobility [$\text{cm}^2 \text{V}^{-1} \text{s}^{-1}$]	
	t_{HT}	t_{HH}	t_{TT}	m_{\parallel}^*/m_0 (column)	m_{\perp}^*/m_0 (transverse)	$\mu_{2\text{-probe,max}}$	$\mu_{4\text{-probe}}$
Ph-DNT-VW	+33	-50	-33	2.3	2.6	3.1	3.0
C₁₀Ph-DNT-VW	+40	-45	-32	2.3	2.7	8.1	8.1
C₁₀-DNT-VW	+43	-69	-35	1.8	2.6	6.5 ²⁰	9.7
DNT-V	+37	-46	-13	3.3 ²⁶	3.3 ²⁶	1.5 ²⁰	1.7

substrate.²⁰ However, at such a temperature, an abrupt decrease in mobility was observed, which was resulted from partial vanishments of the OSC film. We also observed a similar phenomenon with **C₁₀Ph-DNT-VW** in the current study (Figure S24). Thus, an extension of alkyl substituent does not show any remarkable enhancements of thermal durability. On the other hand, **C₁₀Ph-DNT-VW** showed stable thin-film morphology and sufficient crystallinity even after thermal treatment at 180 °C (Figure 6a,b and Figure S22). A single-crystalline **C₁₀Ph-DNT-VW** OFET, where F₄-TCNQ and Au electrodes were deposited after the thermal treatment at 180 °C, exhibited the $\mu_{2\text{-probe}}$ of 3.3 cm² V⁻¹ s⁻¹ (Figure S21), approximately a half of the pristine OFET. Therefore, the thermal treatment at 180 °C is not significantly harmful to **C₁₀Ph-DNT-VW** thin films. If once the thermal treatment was applied in advance of the top-contact electrode preparation, the **C₁₀Ph-DNT-VW** OFET showed good transfer curves against thermal stress up to 180 °C (Figure 6c). It should be noted that an improved OFET performance after 100 °C stress compared to that after 60 °C is likely due to the healed OSC–Au interfaces.^{16, 28} As displayed in Figure 6d, the carrier mobility of **C₁₀Ph-DNT-VW**-based OFET was mostly unchanged with thermal stresses up to 180 °C, indicating enhanced thermal durability compared to **C₆-DNT-VW**. Hence, the alkylphenyl substituents can be advantageous for crystalline OSCs to realize the high thermal durability accompanied by solution processability and high carrier mobility.

Conclusions

In summary, we have developed and investigated the sulphur-containing V-shaped π -electron systems with phenyl substituents. **Ph-DNT-VW** and **C₁₀Ph-DNT-VW** were readily synthesized through a versatile synthetic procedure. Single crystal data and theoretical calculations revealed that both derivatives form typical herringbone-type packing structures that are favourable for two-dimensional charge transport. Single-crystalline OFETs of **Ph-DNT-VW** and **C₁₀Ph-DNT-VW** show excellent mobility of 3.1 and 8.1 cm² V⁻¹ s⁻¹ with band-like transport characteristics. Finally, solution-processable **C₁₀Ph-DNT-VW** exhibit high thermal durability up to 180 °C, which is promising for applicable electronics.

Conflicts of interest

There are no conflicts to declare.

Acknowledgements

This work was supported by the JST-PRESTO programs “Molecular Technology and Creation of New Functions” (grant JPMJPR13K5 and JPMJPR12K2) and “Scientific Innovation for Energy Harvesting Technology” (JPMJPR17R2) and KAKENHI. T.O. and H.I. thank JSPS for a Grant-in-Aid for Scientific Research B (KAKENHI Grant Number JP17H03104 and JP18H01856). The synchrotron X-ray experiment was

performed with the approval of the Photon Factory Program Advisory Committee (Grant No. 2017S2-001).

Notes and references

- Z. Bao and J. Locklin, *Organic Field-Effect Transistors*, 1st ed.; CRC Press: Florida, 2007.
- K. Takimiya, S. Shinamura, I. Osaka and E. Miyazaki, *Adv. Mater.*, 2011, **23**, 4347-4370.
- S. Fratini, M. Nikolka, A. Salleo, G. Schweicher and H. Sirringhaus, *Nat. Mater.*, 2020, **19**, 491-502.
- T. Okamoto, C. P. Yu, C. Mitsui, M. Yamagishi, H. Ishii and J. Takeya, *J. Am. Chem. Soc.*, 2020, **142**, 9083-9096.
- R. A. Marcus, *J. Chem. Phys.*, 1956, **24**, 966-978.
- J. Takeya, K. Tsukagoshi, Y. Aoyagi, T. Takenobu and Y. Iwasa, *Jpn. J. Appl. Phys.*, 2005, **44**, L1393-L1396.
- V. Podzorov, E. Menard, J. A. Rogers and M. E. Gershenson, *Phys. Rev. Lett.*, 2005, **95**, 226601.
- J. Takeya, J. Kato, K. Hara, M. Yamagishi, R. Hirahara, K. Yamada, Y. Nakazawa, S. Ikehata, K. Tsukagoshi, Y. Aoyagi, T. Takenobu and Y. Iwasa, *Phys. Rev. Lett.*, 2007, **98**, 196804.
- A. Troisi, *Chem. Soc. Rev.*, 2011, **40**, 2347-2358.
- S. Illig, A. S. Eggeman, A. Troisi, L. Jiang, C. Warwick, M. Nikolka, G. Schweicher, S. G. Yeates, Y. H. Geerts, J. E. Anthony and H. Sirringhaus, *Nat. Commun.*, 2016, **7**, 10736.
- T. Kubo, R. Haeusermann, J. Tsurumi, J. Soeda, Y. Okada, Y. Yamashita, N. Akamatsu, A. Shishido, C. Mitsui, T. Okamoto, S. Yanagisawa, H. Matsui and J. Takeya, *Nat. Commun.*, 2016, **7**, 11156.
- A. Yamamoto, Y. Murata, C. Mitsui, H. Ishii, M. Yamagishi, M. Yano, H. Sato, A. Yamano, J. Takeya and T. Okamoto, *Adv. Sci.*, 2018, **5**, 1700317.
- T. Uemura, Y. Hirose, M. Uno, K. Takimiya and J. Takeya, *Appl. Phys. Express*, 2009, **2**, 111501.
- G. Giri, E. Verploegen, S. C. Mannsfeld, S. Atahan-Evrenk, D. H. Kim, S. Y. Lee, H. A. Becerril, A. Aspuru-Guzik, M. F. Toney and Z. Bao, *Nature*, 2011, **480**, 504-508.
- J. Soeda, T. Uemura, T. Okamoto, C. Mitsui, M. Yamagishi and J. Takeya, *Appl. Phys. Express*, 2013, **6**, 076503.
- A. Yamamura, S. Watanabe, M. Uno, M. Mitani, C. Mitsui, J. Tsurumi, N. Isahaya, Y. Kanaoka, T. Okamoto and J. Takeya, *Sci. Adv.*, 2018, **4**, eaao5758.
- Y. Shi, L. Jiang, J. Liu, Z. Tu, Y. Hu, Q. Wu, Y. Yi, E. Gann, C. R. McNeill, H. Li, W. Hu, D. Zhu and H. Sirringhaus, *Nat. Commun.*, 2018, **9**, 2933.
- S. Kumagai, A. Yamamura, T. Makita, J. Tsurumi, Y. Y. Lim, T. Wakimoto, N. Isahaya, H. Nozawa, K. Sato, M. Mitani, T. Okamoto, S. Watanabe and J. Takeya, *Sci. Rep.*, 2019, **9**, 15897.
- H. Jiang and W. Hu, *Angew. Chem. Int. Ed.*, 2020, **59**, 1408-1428.
- T. Okamoto, C. Mitsui, M. Yamagishi, K. Nakahara, J. Soeda, Y. Hirose, K. Miwa, H. Sato, A. Yamano, T. Matsushita, T. Uemura and J. Takeya, *Adv. Mater.*, 2013, **25**, 6392-6397.
- Bulletin of the American Group. International Institute for Conservation of Historic and Artistic Works*, 1968, **8**, 20-24.
- H. Klauk, M. Halik, U. Zschieschang, G. Schmid, W. Radlik and W. Weber, *J. Appl. Phys.*, 2002, **92**, 5259-5263.
- H. Ebata, T. Izawa, E. Miyazaki, K. Takimiya, M. Ikeda, H. Kuwabara and T. Yui, *J. Am. Chem. Soc.*, 2007, **129**, 15732-15733.
- T. Yamamoto and K. Takimiya, *J. Am. Chem. Soc.*, 2007, **129**, 2224-2225.

25. T. Okamoto, M. Mitani, C. P. Yu, C. Mitsui, M. Yamagishi, H. Ishii, G. Watanabe, S. Kumagai, D. Hashizume, S. Tanaka, M. Yano, T. Kushida, H. Sato, K. Sugimoto, T. Kato and J. Takeya, *J. Am. Chem. Soc.*, 2020, 10.1021/jacs.1020c05522.
26. C. Mitsui, M. Yamagishi, R. Shikata, H. Ishii, T. Matsushita, K. Nakahara, M. Yano, H. Sato, A. Yamano, J. Takeya and T. Okamoto, *Bull. Chem. Soc. Jpn.*, 2017, **90**, 931-938.
27. W. Gao and A. Kahn, *Appl. Phys. Lett.*, 2001, **79**, 4040-4042.
28. T. Uemura, C. Rolin, T.-H. Ke, P. Fesenko, J. Genoe, P. Heremans and J. Takeya, *Adv. Mater.*, 2016, **28**, 151-155.
29. E. G. Bittle, J. I. Basham, T. N. Jackson, O. D. Jurchescu and D. J. Gundlach, *Nat. Commun.*, 2016, **7**, 10908.
30. C. Liu, G. Li, R. Di Pietro, J. Huang, Y.-Y. Noh, X. Liu and T. Minari, *Phys. Rev. Appl.*, 2017, **8**, 034020.
31. T. Hamai, S. Arai, H. Minemawari, S. Inoue, R. Kumai and T. Hasegawa, *Phys. Rev. Appl.*, 2017, **8**, 054011.
32. G. Horowitz, *J. Mater. Res.*, 2004, **19**, 1946-1962.
33. K. Lee, É. D. Murray, L. Kong, B. I. Lundqvist and D. C. Langreth, *Phys. Rev. B*, 2010, **82**, 081101.
34. P. Giannozzi, S. Baroni, N. Bonini, M. Calandra, R. Car, C. Cavazzoni, D. Ceresoli, G. L. Chiarotti, M. Cococcioni, I. Dabo, A. D. Corso, S. d. Gironcoli, S. Fabris, G. Fratesi, R. Gebauer, U. Gerstmann, C. Gougoussis, A. Kokalj, M. Lazzeri, L. Martin-Samos, N. Marzari, F. Mauri, R. Mazzarello, S. Paolini, A. Pasquarello, L. Paulatto, C. Sbraccia, S. Scandolo, G. Sclauzero, A. P. Seitsonen, A. Smogunov, P. Umari and R. M. Wentzcovitch, *J. Phys.: Condens. Matter*, 2009, **21**, 395502.
35. T. F. Harrelson, V. Dantanarayana, X. Xie, C. Koshnick, D. Nai, R. Fair, S. A. Nuñez, A. K. Thomas, T. L. Murrey, M. A. Hickner, J. K. Grey, J. E. Anthony, E. D. Gomez, A. Troisi, R. Faller and A. J. Moulé, *Mater. Horiz.*, 2019, **6**, 182-191.
36. H. H. Choi, H. T. Yi, J. Tsurumi, J. J. Kim, A. L. Briseno, S. Watanabe, J. Takeya, K. Cho and V. Podzorov, *Adv. Sci.*, 2020, **7**, 1901824.